JCIM JOURNAL OF CHEMICAL INFORMATION AND MODELING

pubs.acs.org/jcim Article

Rotation and Self-Assembly Driving NLRP3 Activation

Haochen Xu, Zhonghuai Hou,* Rongbin Zhou,* and Jie-Lou Liao*

Cite This: J. Chem. Inf. Model. 2024, 64, 6857−6865 Read Online

ACCESS | Metrics & More | Article Recommendations | Supporting Information

ABSTRACT: As a critical sensor protein, NLRP3 detects cellular perturbation caused by diverse exogenous and endogenous stimuli. NLRP3 activation requires domain rotation within the NEK7-bound NLRP3 monomer and assembly. However, a detailed molecular mechanism for NLRP3 assembly and activation remains elusive, particularly in terms of dynamics and energetics. In this work, all-atom molecular dynamics (MD) simulations are executed to describe large-amplitude closed-to-open conformational transitions along the rotational pathway. From the MD trajectories, the computed potential of mean force (PMF) shows that NLRP3 activation through monomeric domain rotation is an uphill process, during which the active conformation of the NLRP3-NEK7 monomer cannot be stabilized. Further binding free-energy calculations for two neighboring NLRP3-NEK7 subunits in a disc assembly with the C10 symmetry reveal that the protein self-assembly starts approximately at the 86.5° position on the rotary pathway, along which the NLRP3 activation becomes a downhill process to the active state at 90.5°. The active NLRP3-NEK7 monomeric conformation in the disc assembly is stabilized because of the interactions between the neighboring subunits, involving mainly FISNA loop 1 in one subunit and a "crocodile-clip" structure formed by the NBD helix-loop-strand motif (residues 351−373) and the WHD β-hairpin loop (residues 501−521) in the other. Our simulations also demonstrate that NEK7 plays an important role in the NLRP3 cage dissociation in the centrosome, which is consistent with biological experiments. The computational results provide kinetic, energetic, and structural insights into the molecular mechanisms of the activation of NLRP3 and the NEK7-driven dissociation of inactive NLRP3 cages. The activation mechanism of NLRP3 proposed in this work is significantly different from those of previous structural studies.

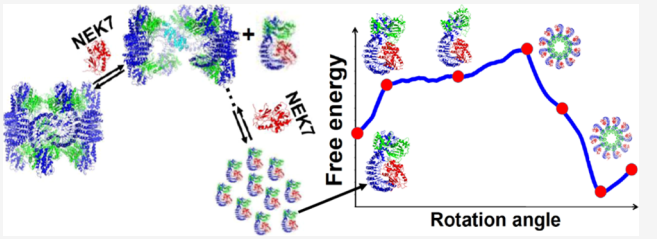

Downloaded via UNIV SCIENCE AND TECHNOLOGY CHINA on October 29, 2024 at 09:39:47 (UTC).
See https://pubs.acs.org/sharingguidelines for options on how to legitimately share published articles.

1. INTRODUCTION

Nucleotide-binding oligomerization domain (NOD)-like, leucine-rich repeat (LRR)-, and pyrin domain (PYD)-containing-3 (NLRP3) is an inflammasome sensor protein that can sense a variety of pathogen-associated molecular patterns (PAMPs) and damage-associated molecular patterns (DAMPs) to regulate the innate immune response.[1−3] As a member of the NLR family, NLRP3 bears a tripartite domain architecture composed of a central NACHT domain, an N-terminal PYD that recruits apoptosis-associated speck-like protein containing a CARD (ASC), and a C-terminal LRR domain that can maintain the protein in its autoinhibitory state. The NACHT domain contains several subdomains, including a FISNA (fish-specific NACHT-associated domain), a nucleotide-binding domain (NBD) that binds and hydrolyzes ATP, helical domain 1 (HD1), a winged helix domain (WHD), and helical domain 2 (HD2)[4] (Figure 1). In contrast to other NLR family members, such as NLR family apoptosis inhibitory proteins (NAIPs) that are activated by well-defined PAMPs, the activation of NLRP3 can be triggered by a wide range of exogenous pathogens and endogenous danger agents.[1,2] Upon stimulation, NLRP3 assembles and recruits the adaptor protein ASC for enlistment of procaspase-1 to form the inflammasome that activates caspase-1. Activated caspases then proteolytically process IL-1β, IL-18, and gasdermin D, leading to inflammatory immune responses and pyroptosis. Aberrant activation of the NLRP3 inflammasome is implicated in a number of diseases, including familial cold autoinflammatory syndrome (FCAS), Muckle-Wells syndrome, neonatal-onset multisystem inflammatory disorder (NOMID), Alzheimer's disease, atherosclerosis, type 2 diabetes, and cancer.[5−8] Therefore, NLRP3 represents a promising drug target that has elicited considerable drug discovery and development efforts. A molecular understanding of the NLRP3 assembly and activation mechanism is thus of great importance for the development of potential therapeutic treatments of related diseases.

As a critical perturbation detector of cellular stress and membrane damage, NLRP3 is the most studied inflammasome sensor.[4] Prior to activation, NLRP3 binds to membrane phospholipids of various intracellular organelles, including the mitochondria, endoplasmic reticulum, and *trans*-Golgi network (TGN). NLRP3 can be activated by many stimuli with

Received: July 1, 2024
Revised: August 9, 2024
Accepted: August 14, 2024
Published: August 27, 2024

ACS Publications © 2024 American Chemical Society

https://doi.org/10.1021/acs.jcim.4c01112
J. Chem. Inf. Model. 2024, 64, 6857−6865

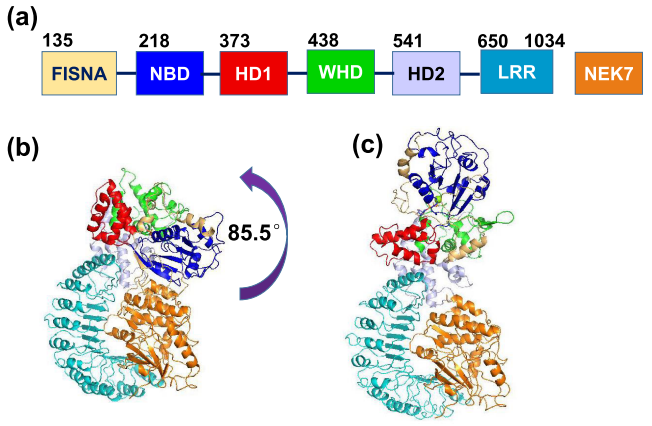

Figure 1. (a) Domain organization of the human NLRP3-NEK7 monomer with labeled domain boundary and colored light orange, blue, red, green, light blue, cyan, and orange for FISNA, NBD, HD1, WHD, HD2, LRR, and NEK7, respectively, in (b) the inactive conformation at 5° and (c) the active conformation of NLRP3 at 90.5°.

extensive chemical and structural diversity. These stimuli include bacterial toxins, such as nigericin, extracellular ATP, and particulates, such as uric acid crystals, cholesterol crystals, and amyloids. The mechanisms of action of these stimuli often converge on potassium efflux or other ionic changes.[9−11] In addition, several research groups have identified a centrosomal serine/threonine kinase NEK7 (Never In Mitosis A-related kinase 7) as an essential component that licenses NLRP3 activation.[12−14] It was suggested that upon stimulation, NLRP3 is further transported into the centrosome, also known as the microtubule-organizing center (MTOC), where NEK7 is located.[15−17] In the MTOC, NLRP3 interacts with NEK7 and assembles into an active inflammasome.

In recent years, significant progress has been made in the determination of full-length cryo-EM NLRP3 structures.[18−24] The first full-length NLRP3 structure, which was engineered to be monomeric, was determined in complex with NEK7 (PDB: 6NPY).[18] On the basis of the 6npy inactive structure, a dynamic model was proposed to describe the transition from the inactive (PDB: 6npy) to active conformation of the NLRP3-NEK7 monomer using NLRC4 as a homology reference.[18] In this hypothetical model, a ∼90° rotation of the NBD-HD1 module relative to the immobile WHD-HD2-LRR module complexed with NEK7 was generated to achieve the active conformation along an axis at the junction between HD1 and WHD, starting from the 6npy structure. However, the hypothetical active structure thus obtained for the NLRP3-NEK7 monomer has not been observed in experiments so far but instead was determined in the decameric disk assembly from a recent cryo-EM experiment.[22]

In its native form, NLPR3 often forms an oligomeric double-ring cage structure,[19] in which each NLRP3 monomeric subunit adopts a conformation slightly different from the 6npy structure. As shown in a dodecamer mouse NLRP3 structure (PDB: 7LFH), six of 12 NATCH domains are arranged in the top and down surfaces without close interactions with each other, whereas 12 LRR domains form the lateral side of the cage via back-to-back and face-to-face interactions between neighboring LRR domains, contributing the most to the cage formation.[19] A decameric human NLRP3 cage has also been determined recently in a cryo-EM study (PDB code: 7pzc).[20] Although the exact oligomeric state varies with bound ligands, all of those NLRP3 oligomers determined thus far bear the double-ring architecture formed by the LRR−LRR interactions similar to that in the 7LFH or 7PZC structure.[4]

An inactive double-ring cage structure seems to be required for the conversion of an NLRP3-activating signal to the trans-Golgi network (TGN) dispersion, as this type of structure can avoid premature activation before NLRP3 is transported to MTOC.[19] Intriguingly, the concave side of the LRR domain provides a binding site not only for the neighboring LRRs to form the cage but also for NEK7 binding. It has been proposed from biological experiments that when NLRP3 is transported to the centrosome where NEK7 is located, NEK7 binds to the LRR and disrupts the LRR−LRR interface, leading to the cage dissociation.

A recent cryo-EM study demonstrates that active NLRP3 forms a 10-subunit (PDB: 8ej4) or 11-subunit disk conformation complexed with NEK7.[22] Overlay of an inactive NLRP3-NEK monomer (PDB: 6npy) and the active one taken from the 8ej4 decameric disk shows that the inactive NLRP3 monomer assumes a closed conformation, in which the FISNA-NBD-HD1 module is in close contact with the WHD-HD2-LRR region in complex with NEK7, whereas the active protein adopts an open conformation where the FISNA-NBD-HD1 head already departs from the WHD-HD2-LRR-NEK7 body (Figure 1). The structural alignment demonstrates that the active FISNA-NBD-HD1 module is found to rotate by 85.5° along the axis at the junction between HD1 and WHD, allowing the protein to transition from the inactive to the active conformation.

Based on previous structural studies, a possible NLRP3 activation process was proposed to include the steps as follows.[9,22] After priming and upregulation of NLRP3 expression, the NLRP3 oligomeric cage is formed in the *trans*-Golgi network (TGN). Upon stimulation, TGN dispersion into vesicles occurs, and NLRP3 is further transported into MTOC. In the MTOC, the inactive NLRP3 cage is dissociated into two half-rings via interacting with NEK7. After the cage dissociation, the fully active NLRP3 disk would possibly be formed by these two half-rings.[22] However, as the conformation of an inactive NLRP3 half-ring is significantly different from that of the active disc assembly, how NLRP3 can undergo a large-amplitude conformational transition in such a large protein complex is questionable. In particular, as the transition from an inactive to an active state is highly dynamic, a molecular understanding of how the NLRP3 protein is activated in terms of dynamics and energetics remains elusive. For this purpose, all-atom molecular dynamics (MD) simulations are executed to compute the free-energy profile along the activation pathway in this work. Our simulation results provide a rationale for NLRP3 assembly and activation.

2. MATERIALS AND METHODS

2.1. Enforced-Rotation MD Simulations and PMF Calculations. The monomeric NLRP3 structure taken from the cryo-EM cage of inactive human NLRP3 (PDB: 7pzc)[20] was used to form an NLRP3-NEK7 complexed monomer (see the text in the Supporting Information, SI) as the starting point for MD simulations in this work. The missing residues were modeled using the loop module in the SYBYL-X2.1.1 package. This monomeric complex, in which the nucleotide ligand (MgADP) remains in the nucleotide-binding site, was inserted

https://doi.org/10.1021/acs.jcim.4c01112
J. Chem. Inf. Model. 2024, 64, 6857−6865

into an 11 × 11 × 14 nm^3 box with a minimum distance of 1.5 nm between the protein and the box boundary and solvated with TIP3P water molecules at the physiological ionic concentration of 0.15 M NaCl. Periodic boundary conditions were applied in all directions. The amber99sb-ildn force field[25] was used for the protein and ions. Ligand topology, atom typing, and assignment of bonded parameters for the nucleotide ligand (MgADP or MgATP) were performed with the general amber force field (gaff).[26] Long-range electrostatic interactions were treated with the particle mesh Ewald (PME) method with a real-space cutoff of 1 nm and a Fourier grid spacing of 0.1 nm.[27] Short-range Lennard−Jones interactions were cut off at 1.2 nm, and the LINCS[28] constraints were used for bond lengths of proteins and ligands and SETTLE[29] for water molecules.

All molecular dynamics (MD) simulations in this work were performed with a 2 fs time step using the GROMACS 2018.4 package with GPU acceleration.[30] Energy minimization was performed using the steepest descent method of 50,000 steps to release conflicting contacts. Following the steepest descent minimizations and applying the position restraints on peptide heavy atoms, the system was equilibrated by 100 ps MD simulations with NVT using the V-rescale coupling thermostat,[31] followed by 1 ns MD simulations with NPT using the Nose−Hoover thermostat[32] and the Parrinello−Rahman barostat[32] to maintain temperature at 298 K and pressure at 1.0 bar. Then, the system was equilibrated for 50 ns at 298 K and 1 bar prior to the enforced rotation of the protein.

Starting from the above equilibrated NLRP3-NEK7 system, an enforced-rotation MD method[33] was applied in the following simulations. In this method, all 305 C_α atoms of FISNA, NBD, and HD1 were chosen as the rotation group. The axis at the junction between HD1 and WHD was used as the rotation vector. The pivot vector of the axis was placed at the C_α atom of Ala441.[22,34] To simulate the rotation of the FISNA-NBD-HD1 module (rotor) relative to the WHD-HD2-LRR-NEK7 module, the backbone atoms were harmonically restrained to their initial positions. The rotor was then driven in active direction,[18] at an angular rate of 0.1°/ns during 0.9 μs of simulation time with the spring constant of 1000 kJ/(mol·nm^2). This yielded a 90° rotation, which covers a complete conformational activation process.

To compute the potential of mean force (PMF) along the rotational pathway, a weighted histogram analysis method (WHAM)[35] with umbrella sampling[36] was applied. Structural snapshots were taken from the above enforced-rotation MD trajectory to generate 251 configurations for the umbrella sampling simulations. In each window, 50 ns MD umbrella sampling simulations were performed, resulting in a total simulation time of 12.5 μs. The PMF along the rotational pathway was then obtained using the WHAM analysis for evaluating the data from a series of umbrella sampling.

2.2. Binding Free-Energy Calculations Using the Screening MM/PBSA Method. To calculate the free energy of protein−ligand (including NLRP3-NLRP3 and NLRP3-NEK7) binding, an improved version for the standard molecular mechanics (MM)/Poisson−Boltzmann (PB) surface area (MM/PBSA) method (named the screening MM/PBSA)[37] was applied in this work. The protein−ligand binding free energy (ΔG_{bind}) is written as[38]

$$\Delta G_{bind} = \Delta H - T\Delta S = \Delta E_{MM} + \Delta G_{SOL} - T\Delta S \quad (1)$$

where ΔH and ΔS are the changes in enthalpy and entropy, respectively, and T is the absolute temperature. The protein binding free energy ΔG_{bind} can be decomposed into the changes of gas-phase molecular mechanics (MM) energy ΔE_{MM}, solvation free energy ΔG_{sol}, and the contribution $T\Delta S$ from the conformational entropy ΔS, which is calculated using the interaction entropy method efficiently.[39,40]

In eq 1 ΔE_{MM} and ΔG_{sol} are given, respectively, by

$$\Delta E_{MM} = \Delta E_{int} + \Delta E_{ele} + \Delta E_{vdW} \quad (2)$$

$$\Delta G_{sol} = \Delta G_{PB} + \Delta G_{SA} \quad (3)$$

$$\Delta G_{SA} = \gamma \mathrm{SASA} + b \quad (4)$$

Here, ΔE_{int}, ΔE_{ele}, and ΔE_{vdW} are the changes of the internal energy, the electrostatic energy, and the van der Waals interaction energy, respectively. In eq 3, ΔG_{sol} includes the electrostatic solvation energy ΔG_{PB}, which comes from the polar contribution, and ΔG_{SA} from the nonpolar contribution (between the solute and the continuum solvent). While the polar contribution ΔG_{PB} can be computed with the PB method, the nonpolar term ΔG_{SA} is often evaluated using the solvent-accessible surface area (SASA) given in eq 4, where γ is the surface tension coefficient of 2.27 kJ/(mol·nm^2), and b is a constant with the value of 3.85 kJ/mol.[37,41]

In the screening MM/PBSA method, ΔE_{ele} in eq 2 is written as[36]

$$\Delta E_{ele} = \sum_i \sum_j \frac{q_i q_j}{4\pi\varepsilon_0\varepsilon_{in} r_{ij}} e^{-r_{ij}/\lambda_D} \quad (5)$$

where q_i and q_j are the charges of atom i and j, respectively, in the two proteins, r_{ij} is the distance between atom i and j, ε_0 and ε_{in} in eq 4 are the permittivity in vacuum and the relative permittivity of the solute (i.e., protein), respectively, and λ_D is the electrostatic screening length, which can be expressed as

$$\lambda_D = \sqrt{\varepsilon_0\varepsilon_{out} k_B T / e^2 \sum_i c_i z_i^2} \quad (6)$$

Here, ε_{out} is the permittivity of the solvent (i.e., water, $\varepsilon_{out} \sim 80$), k_B is the Boltzmann constant, e is the electron charge, c_i and z_i are the concentration and charge of the i-th ion, respectively. The default values, $\varepsilon_0 = 1$, $\varepsilon_{in} = 2$, and $\lambda_D = 8$ Å, were used.[37] This modified MM/PBSA method has shown much better performance, particularly for highly charged protein systems, than the standard MM/PBSA.[37,41]

The above screening MM/PBSA method was applied to calculate the NLRP3-ligand binding free energies using all-atom molecular dynamics (MD) simulations of the protein−ligand complex with an explicit solvent model in this work. The single trajectory protocol was applied for the protein complex, by which a single MD trajectory was obtained to extract the structural snapshots of all components of the protein complex. The last 5 ns of each 50 ns equilibrated MD trajectory described above was used with an interval of 100 ps, resulting in 51 frames for each run using the screening MM/PBSA method. The gmx_mmpbsa script (https://jerkwin.github.io/gmxtool), together with the APBS program,[42] was employed to compute the binding free energy and its energy decomposition terms such as the electrostatic energy, the van der Waals energy, and the solvation energy including the polar and nonpolar parts.

https://doi.org/10.1021/acs.jcim.4c01112
J. Chem. Inf. Model. 2024, 64, 6857−6865

3. RESULTS AND DISCUSSION

3.1. Free-Energy Profile along the Rotational Pathway for the NLRP3 Monomer. To investigate the free-energy profile for the inactive to active conformational transition of an NLRP3-NEK7 monomer, we calculated the free energies along the rotational pathway proposed previously[18] from 5 to 95°. The initial inactive structure was extracted from the cryo-EM cage structure of inactive human NLRP3 (PDB: 7pzc)[18] to form the NLRP3-NEK7 monomeric complex at θ = 5° (see SI text, Figures S1−S4). To this end, we executed a 0.9-μs rotation simulation (see Movie in the SI), from which 251 configurations were obtained. In the simulations, all 305 C_α atoms of the FISNA-NBD-HD1 module were chosen as a rotation group, whereas the remaining parts of the complex remained immobile. The weighted histogram analysis method (WHAM) was then used with umbrella sampling[35,36] to obtain the free energy changes ΔG (also termed potential of mean force, PMF) along the rotational pathway.

The resulting PMF versus rotational angle θ is displayed in Figure 2. As shown in this figure, initially, the free energy goes up steeply to ∼10.0 kcal/mol as θ changes from 5 to 18°, after which the PMF rises up relatively slowly to ∼17.2 kcal/mol at 95°. From the above MD trajectories, several snapshots at 5, 20, 50, 80, and 90.5° were extracted, among which the 5 and 90.5° conformations of the NLRP3-NEK7 monomer are shown in Figure 1b,c, respectively. These structural snapshots demonstrate that the NLRP3 monomer executes a transition from the closed conformation at 5°, which is similar to that reported in the 6npy PDB file (Figure S4), to the open conformation at 90.5°, which corresponds to the one in the active assembled disk (PDB: 8ej4).[22] In the initial 5° structure, the mobile domains are in the closest contact with the immobile WHD-HD2-LRR-NEK7 module. Subsequently, these two parts depart gradually from each other along the rotational pathway.

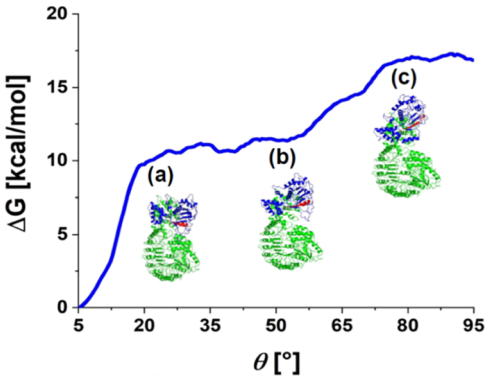

Figure 2. Free energy changes ΔG along the rotational pathway of the NLRP3 monomer (blue solid line). The conformations from simulations are shown at (a) 20°, (b) 50°, and (c) 80°, respectively. To show the rotary motion of the FISNA-NBD-HD1 module (blue) relative to the immobile WHD-HD2-LRR-NEK7 module (green), an NBD helix-loop-strand motif (residues 351−373) in the mobile NBD head is highlighted red.

The total contact areas between the mobile and immobile modules were also calculated as a function of rotational angles and are displayed in Figure 3a. As shown in this figure, the contact area decreases gradually as θ is increased, qualitatively consistent with the calculated PMF (Figure 2). The contact area is then decomposed into the contributions of the FISNA-NBD-HD1 module with WHD, HD2, LRR, and NEK7, respectively, displayed in Figure 3b. The results show that during the 5 → 18° process, while the contact between the mobile module and WHD remains almost constant, the contact area of the mobile FISNA-NBD-HD1 module with NEK7 as well as HD2 and LRR decreases significantly, making a major contribution to the increase in the free energy. In the range of 18−55°, the contact area between FISNA-NBD-HD1 and WHD is increased. Interestingly, this increased area is offset approximately by the decreased area between the mobile module with HD2 and LRR at each rotational angle; thereby, the total contact area remains almost unchanged from 18 to 55° (Figure 3a), after which the mobile-immobile contact area is decreased. As shown in Figure 3b, NEK7 contributes almost nothing to the free-energy profile along the rotational pathway when $\theta \geq 20°$, as the contact area of NEK7 with FISNA-NBD-HD1 already decreases almost to zero. In addition, MgADP binds tightly into the NBD pocket in the mobile module of the 5° NLRP3 monomer but only with a β-phosphate oxygen H-bonded to H522 in the WHD of the immobile module, stabilizing the initial 5° inactive conformation (Figure S5). However, this H-bond is readily broken as θ is increased to 10°, after which MgADP has no significant contribution to the free-energy profile along the rotational pathway.

The overlay of the 90.5° monomeric NLRP3-NEK3 structure extracted from our simulations with the one from the cryo-EM active disk[22] shows structures similar to each other. However, this active monomeric conformation (∼90.5°)

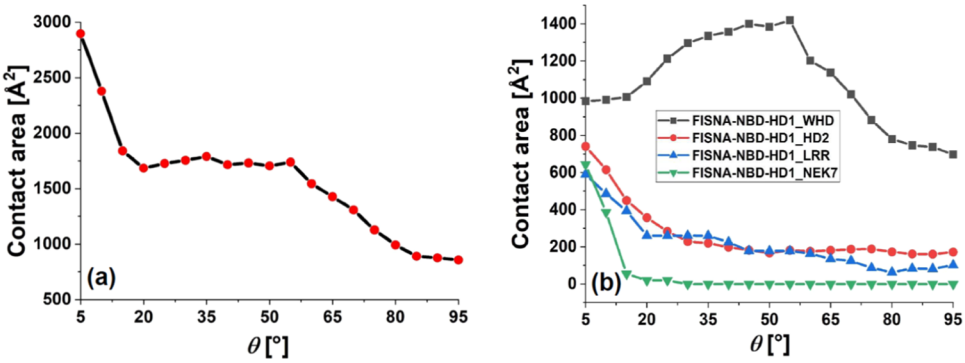

Figure 3. Contact areas of the mobile FISNA-NBD1-HD1 module with (a) the immobile WHD-HD2-LRR-NEK7 module and (b) WHD (solid square, black), HD2 (solid circle, red), LRR (solid triangle, blue), and NEK7 (inverted triangle, green), respectively, versus rotational angles.

https://doi.org/10.1021/acs.jcim.4c01112
J. Chem. Inf. Model. 2024, 64, 6857−6865

from our simulations is energetically unfavorable (16.8 kcal/mol) compared to the inactive one at 5° (see Figure 2), while the contact areas between the mobile and immobile modules are also shown to be 890 and 2850 Å^2, respectively, in the 90.5 and 5° cases (Figure 3a). Our computational results are consistent with the fact that no active monomeric structure has been observed in structural experiments. This raises the question of how to stabilize the active monomeric conformation during NLPR3 activation.

3.2. Binding Free-Energy Profile along the Rotational Pathway for NLRP3 Assembly and Activation. As discussed earlier, NLRP3 forms an inactive cage assembly in the resting state, and upon stimulation, the NLRP3 cage is transported into the centrosome, where NEK7 resides. From our calculations, the total free energy (−142.9 kcal/mol) of NEK7 binding to NLRP3* at 5° (see eq S6 in the SI) is 26.0 kcal/mol lower than the total free energy (−116.9 kcal/mol) of the NLRP3 cage (see eq S4 in the SI) relative to the 10-NLRP3* state (see eq S5 in the SI). The result supports the proposal that NEK7 binding drives the dissociation of the cage assembly and leads to the formation of the NLRP3-NEK7 complexed monomers.[4,19,22] On the basis of our calculations and the cage structure, a kinetic model was proposed for the NEK7-driven dissociation of the inactive NLRP3 cage (see the SI text, eqs (S11−S15) and Figure S6). In this kinetic model, the NLRP3 monomers of the cage assembly are dissociated one by one through the breaking of the face-to-face contacts and the NLRP3(0°) → NLRP3(5°) conformational transition upon binding of NEK7, which drives a population shift toward the product state of the NLRP3(5°) − NEK7 complexed monomers.

Starting from the configuration at θ = 5°, NLRP3 activation requires large rotational movements of the FISNA-NBD-HD1 module by ∼85.5° relative to the WHD-HD2-LRR region, as discussed above. This is an uphill and energetically unfavorable process for the monomeric protein (Figure 2). In principle, an NLRP3-NEK7 monomeric conformation at any rotary angle (θ) could exist in the centrosome but with a probability ρ obeying the Boltzmann equilibrium distribution, i.e., $\rho(\Delta G) \sim e^{-(\Delta G/k_B T)}$. Here, ΔG, k_B, and T are the free energy change, the Boltzmann constant, and temperature, respectively. As shown in Figure 2, the concentration of the NLRP3-NEK7 monomer at a rotational angle ($\theta \gg 0$), for instance, θ = 90.5° would be extremely low compared to that at the initial state θ = 5° owing to the intrinsic low affinity of the domain interactions, as the ratio of $\rho[\Delta G(\theta = 90.5°)]$: $\rho[\Delta G(\theta = 5°)] \cong 10^{-12}$ at T = 298 K. Nevertheless, this scenario can be changed as the NLRP3-NEK7 monomers approach each other for self-assembly during the activation process. This proximity-driven mechanism for assembly and activation was proposed for intracellular higher-order signaling machines more than a decade ago from a structural biology viewpoint.[43] However, studies in terms of dynamics and energetics are still lacking.

To understand how the NLRP3-NEK7 monomeric conformation (Figure 2) is stabilized during the activation of the protein in this work, a cooperative self-assembly mechanism was proposed based on recent structural observations discussed above.[4,24] In this work, the active decameric structure (PDB: 8ej4) with the C10 symmetry[22] was used as the reference. Generated from the MD simulations described above, the NLRP3-NEK7 monomers with different rotary angles (Figure 2) were obtained. A disk structure was assembled, each containing 10 NLRP3-NEK7 subunits with the same rotary angle θ to maintain the C10 symmetry of the disk. Intriguingly, the results have shown that only $\theta \geq 80°$ along the activation pathway could the disk be assembled structurally, while the rotational angle is smaller than 80°, the NLRP3-NEK7 monomer would have a steric clash with its neighbors in the assembly. We then calculated the binding free energy of each monomer binding to its two neighbors in a possible assembled disk along the activation pathway (SI text). The average binding free energy, $\Delta G_B(\theta)$, for an NLRP3-NEK7 monomer was thus obtained (Figure 4). As shown in Figure 4, $\Delta G_B(\theta)$ decreases as the rotary angle θ is increased to θ = 90.5°, after which it goes up with the increase of θ up to 95°.

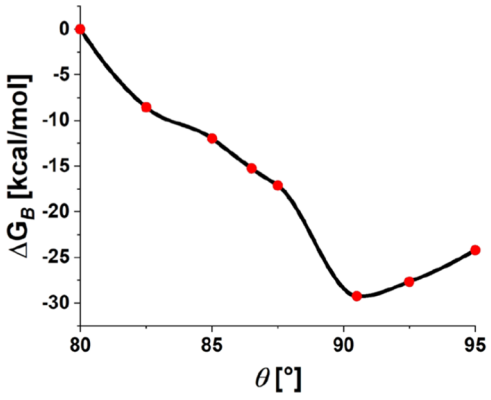

Figure 4. Averaged binding free energy $\Delta G_B(\theta)$ for an NLRP3-NEK7 monomer as a function of rotary angle θ.

To better understand the binding free-energy profile, we examined three representative structures of the NLRP3 assembly at (a) 85°, (b) 90.5°, and (c) 95°, respectively (Figure 4). Overlay of the assembled structure at 90.5° from our simulations to the 8ej4 active disk leads to a root-mean-square deviation (RMSD) of 1.6 Å (Figure S7). As shown in the calculated 90.5° disk structure (Figure 5a), two

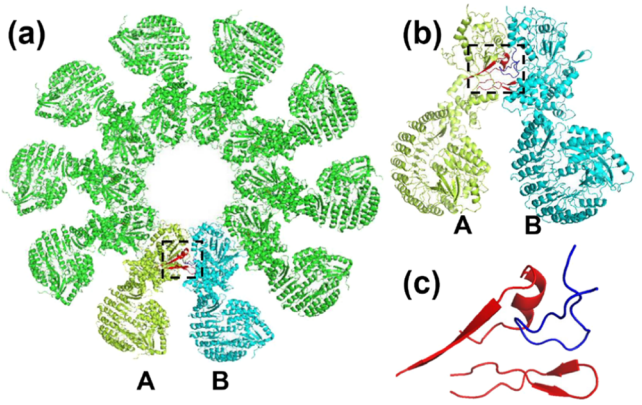

Figure 5. (a) Active NLRP3 disk structure (90.5°) from simulations. (b) Both the NBD helix-loop-strand motif (residues 351−373) and the WHD β-hairpin loop (residues 501−521) in monomer A (limon) are colored red, and the FISNA loop 1 (residues 148−166) of the B monomer (cyan) is colored blue shown in a dashed square. (c) A "crocodile-clip" structure (red) formed by the above NBD helix-loop-strand motif and WHD β-hairpin loop in the A subunit and FISNA loop 1 (blue).

https://doi.org/10.1021/acs.jcim.4c01112
J. Chem. Inf. Model. 2024, 64, 6857−6865

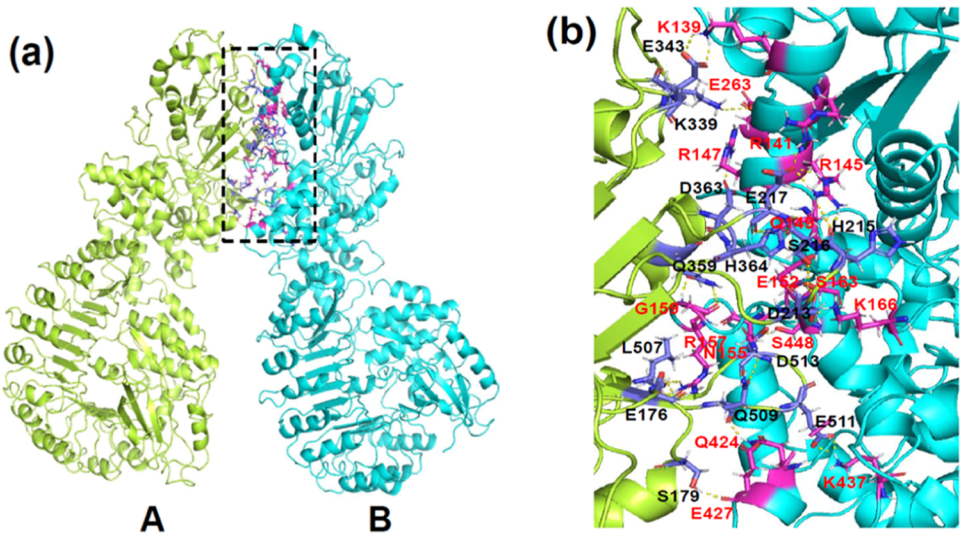

Figure 6. (a) Dimer formed by subunits A (limon) and B (cyan) taken from the 90.5° NLRP3 disk assembly. H-bonds at the A−B interface shown in the dashed-line box are also described in detail in (b). These H-bonds are formed by residues from A (labeled black) and B (red), respectively.

neighboring subunits (labeled A and B) bind to each other tightly, with a contact area of ∼1864 Å^2. In this active conformation, an opened "crocodile-clip" (Figure 5) is formed by an NBD helix-loop-strand motif (residues 351−373) and a WHD β-hairpin loop (residues 501−521) in the A subunit. While this WHD β-hairpin loop extends into a pocket formed by HD1, WHD, and HD2 in the B subunit, FISNA loop 1 in the B subunit binds tightly into the crocodile-clip pocket of the A subunit. Importantly, a number of hydrogen bonds (H-bonds) are formed at the NLRP3- NLRP3 interface in the active (90.5°) disk assembly (Figure 6). Despite the fact that their overwhelming majority are solvent-exposed, these H-bonds make a significant contribution to the binding free energy displayed in Figure 4.

Structural examinations show that both 85 and 95° assemblies bear a similar "crocodile-clip" conformation (Figure S10), into which FISNA loop 1 of subunit B binds in a way similar to that in the active (90.5°) disk assembly. Further structural analysis also demonstrates that the neighboring NLRP3 monomers in these two disks bind to each other in a mode similar to that in the active (90.5°) disk. As shown in Figures 4 and 5, in such a binding mode, NEK7 and LRR of an NLRP3 monomer do not interact with its neighboring subunit in the assembly. In spite of the similarity of binding, the H-bond numbers at the NLRP3 interfaces in the 85° and 95° disks are both obviously less than that in the active (90.5°) assembly owing to slightly different orientations of the corresponding NLRP3 interfaces (Figures S11−S13). Our above analysis provides a rationale for the binding free-energy profile shown in Figure 4.

The binding of B-subunit FISNA loop 1 into the crocodile-clip of the A subunit (Figure 5c) is a characteristic of the assembly process for NLRP3 activation, as shown in the 85, 90.5, and 95° assemblies. For example, in the 90.5° disk assembly, the FISNA loop-1 residues R147, E152, N155, R157, and G159 form H-bonds, respectively, with the crocodile-clip residues D363, H364, Q509, E176, and Q359, contributing significantly to the NLRP3-NLRP3 binding free energy for the assembly. The crocodile-clip structure in an NLRP3-NEK7 monomer starts to form around θ = 55°, but the pocket space in the crocodile-clip is relatively small compared to that in the active conformation when θ < 80°(Figures S9 and S10). For example, in a 75°disc structure constructed with the 8ej4 active disk as a reference, FISNA loop 1 of the B subunit would clash with the NBD helix-loop-strand motif of the A subunit, as the pocket in the crocodile-clip is relatively small compared to that in the active conformation. Such clashes would prevent two NLRP3-NEK7 subunits from forming a dimer for the disc assembly, which leads to activation. Only when the NLRP3-NEK7 monomer rotates by a degree larger than 80° does the crocodile-clip pocket become more open for the accommodation of FISNA loop 1 from its neighboring subunit, allowing for the formation of the assembly.

Besides the structural constraint discussed above, however, a free energy restraint for a meaningful assembly leading to NLPR3 activation is also required. For example, the binding free energy between two neighboring NLRP3-NEK7 subunits in the 80° assembly can be negligible (Figure 4), the averaged free energy for an NLRP3-NEK7 subunit in the assembly (relative to that at 5°) is 16.94 kcal/mol (Figure 7), which

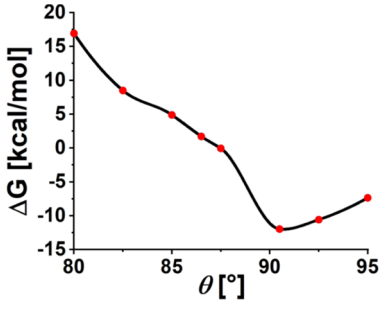

Figure 7. Free energy ΔG for an NLRP3-NEK7 subunit in the disk assembly as a function of the rotary angle θ.

equals that of the NLRP3(80°)-NEK7 monomer shown in Figure 2. Therefore, the total free energy for an 80° decameric disk $[(\text{NLRP3}(80°) - \text{NEK7})_{10}]$ would be 169.4 kcal/mol. This free energy is obviously too large, suggesting that the 80° assembly may not be on the activation pathway. Interestingly, the averaged binding free energy of an NLPR3-NEK7 subunit in the 86.5° decameric disk is −15.26 kcal/mol, as shown in

https://doi.org/10.1021/acs.jcim.4c01112
J. Chem. Inf. Model. 2024, 64, 6857−6865

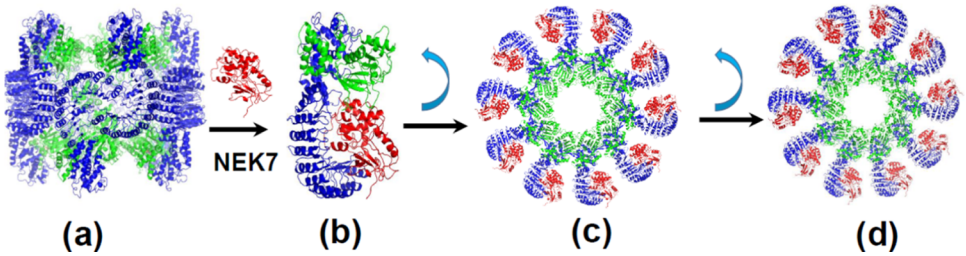

Figure 8. Proposed model for NLRP3 assembly and activation. (a) Inactive NLRP3 decameric cage. (b) Inactive NLRP3-NEK7 monomer at 5°. (c) Inactive NLRP3-NEK7 disk at 86.5°. (d) Active NLRP3-NEK7 disk at 90.5°.

Figure 4. In this case, the averaged free energy of an NLRP3-NEK7 subunit is thus reduced from 16.96 kcal/mol (Figure 2) to 1.70 kcal/mol. Therefore, the total free energy of the 86.5° decameric assembly is 17.0 kcal/mol, which is almost equal to the free energy (16.96 kcal/mol) of the corresponding NLRP3-NEK7 monomer (Figure 2). From these computational results, we propose that the NLRP3 self-assembly starts approximately at the 86.5° position on the assembly and activation pathway.

3.3. Molecular Mechanism for NLRP3 Assembly and Activation. Along the rotary pathway ($\theta \geq 80°$), the overall free energy for an NLRP3-NEK7 monomer in a disc assembly is the summation of the free energy (PMF) and the binding free energy displayed in Figures 2 and 4, respectively. Therefore, the free energy for an NLRP3-NEK7 subunit in the disk structure was obtained along the rotary pathway displayed in Figure 7. As seen in Figure 7, the NLRP3 assembly and activation is a downhill process starting from θ = 86.5° up to 90.5° on the rotational pathway, along which the free energy of the NLRP3-NEK subunit is reduced compared to that of the corresponding monomer (Figure 2) due to the binding of two neighboring subunits.

On the basis of our simulation results shown in Figures 2 and 7, we propose a model for NLRP3 assembly and activation as follows. Upon stimulation, the inactive NLRP3 cage is transported into the MTOC to engage NEK7 in the centrosome. After NEK7 binding, the NLRP3 cage is dissociated, and the NLRP3-NEK7 complexed monomers (θ = 5°) are formed (see detailed discussion for NEK7-driven dissociation of the inactive NLRP3 cage in SI text and Figure S6). These NLRP3-NEK7 monomers can be thermodynamically activated along the rotational pathway from θ = 5° to θ = 86.5°, at which the monomers start to assemble into an inactive decameric disk with the C10 symmetry. Subsequently, the FISNA-NBD-HD1 modules of all subunits in the disc assembly rotate synchronously relative to the immobile parts (WHD-HD2-LRR-NEK7) until the active disk assembly is formed at 90.5°. As shown in Figure 7, the NLRP3 assembly starting from θ = 86.5° is a downhill process until θ = 90.5° where a free energy minimum is reached. The model proposed here is significantly different from that suggested in biological structural studies,[18,22] as shown in Figure 8 (see Figure S6 in the SI for the first step).

In the above model from our simulations, NEK7 is essential in the dissociation of the inactive NLRP3 cage but apparently has no significant effect on the assembly and activation process, as NEK7 binds to neither the mobile module in the NLRP3 monomer ($\theta \geq 20°$, Figure 2) nor neighboring NLRP3-NEK7 subunits in the assembly ($\theta \geq 86.5°$, Figure 4). Our computational results related to the roles of NEK7 in the NLRP3 activation as well as in the dissociation of the inactive cage are qualitatively consistent with the experiments.[4,18−22]

4. CONCLUSIONS

NLRP3 inflammasome is an important perturbation detector for cellular stress and damage. Activation of NLRP3 as the inflammasomal sensor has a critical role in the formation of the inflammasome complex for the release of cytokines IL-1β, IL-18, and pyroptosis. As demonstrated in biological experiments, NLRP3 activation is performed through the intramonomeric rotation as well as the direct binding of NEK7.[4] However, NLRP3 cannot be activated by the rotary motion of an NLRP3-NEK7 monomer alone. Instead, NLRP3 activation requires a high-order protein assembly,[43] as shown in structural studies.[4,22] Despite significant advances in biological research over the past years, a mechanistic understanding of the NLRP3 assembly and activation remains incomplete.

In this work, all-atom molecular dynamics simulations were executed to describe the closed-to-open transition process in detail, starting from the 5° inactive conformation to the active (90.5°) conformation of the NLRP3-NEK7 monomer. The PMF calculations show that this monomeric transition is an uphill process along the rotational pathway, on which the active and open conformation (90.5°) of the NLRP3-NEK7 monomer cannot be stabilized by the interdomain interactions and binding of ligands such as NEK7 and nucleotide (MgADP, see Figure S5 and SI text). Our further binding free-energy simulations demonstrate that when $\theta \geq 86.5°$ along the activation pathway, NLRP3-NEK7 monomers start to assemble a decameric disk-like structure, of which C10 symmetry is conserved during the activation process. The resultant free-energy profile shows that the NLRP3 assembly and activation is a downhill process, along which from the barrier at the 86.5° position to the active state (90.5°), the averaged free energy of an NLRP3-NEK7 subunit can be significantly reduced owing to its binding of two neighboring subunits in the disk. The simulation results in this work also unveil that the crocodile-clip structure suitable for FISNA loop-1 binding is a critical structural determinant in the assembly and activation process. Tight binding of FISNA loop-1 into the crocodile-clip pocket is an important characteristic of NLRP3 activation. The free-energy calculations for LRR binding with NEK7, as well as with LRR from another NLRP3 subunit, offer kinetic insight that NEK7 is essential in the dissociation of the inactive cage structure (see the SI text). However, NEK7 has no important role in the assembly and activation as it interacts neither with the mobile domains in the NLRP3-NEK7 monomer nor with the neighboring subunits during the activation process, which is consistent with biological experiments.

https://doi.org/10.1021/acs.jcim.4c01112
J. Chem. Inf. Model. 2024, 64, 6857−6865

The free-energy profiles shown in Figures 2 and 7 suggest a molecular mechanism for the NLRP3 activation, according to which after the NLRP3 inactive cage in the centrosome is dissociated into the NLRP3(5°) monomers complexed with NEK7, these monomers can be thermodynamically activated along the rotary pathway up to about 86.5°, after which the self-assembled disk is formed with the C10 symmetry. Subsequently, all NLRP3-NEK7 subunits in the assembly rotate cooperatively to maintain the C10 symmetry of the disk, and the decameric disk proceeds downhill to the active conformational state at the 90.5° position on the activation pathway. Our free energy computations with all-atom MD simulations provide kinetic, energetic, and structural insights into NLRP3 assembly and activation.

■ ASSOCIATED CONTENT

Data Availability Statement

We have used the GROMACS2018.4 MD simulation package to perform all the simulations. The software can be found at https://www.gromacs.org/index.html. The data analysis has been carried out using gmx_mmpbsa. Analysis codes are available at https://github.com/reborn181/NLRP3.

Supporting Information

The Supporting Information is available free of charge at https://pubs.acs.org/doi/10.1021/acs.jcim.4c01112.

Preparation of the initial NLRP3-NEK7 inactive monomeric structure; NEK7-driven dissociation of the inactive NLRP3 cage assembly; binding free-energy calculations; kinetic model for NEK7-driven dissociation of the inactive NLRP3 cage; and NLRP3-NEK7 disk assemblies (PDF)

Archive file with data in machine-readable formats, including the NLRP3-NEK7 monomeric structures at 5, 20, 80, and 90.5°; the dimeric structures at 85, 90.5, and 95°, in which the hydrogen bonds at the NLRP3 interface are determined, the disk assemblies at 80 and 90.5°, and the movie for NLRP3-NEK7 rotation obtained from the all-atom MD simulations in this work (ZIP)

■ AUTHOR INFORMATION

Corresponding Authors

Zhonghuai Hou − *Department of Chemical Physics, University of Science and Technology of China, Hefei, Anhui 230026, China; Hefei National Research Center for Physical Sciences at the Microscale, University of Science and Technology of China, Hefei, Anhui 230026, China;* orcid.org/0000-0003-1241-7041; Email: hzhlj@ustc.edu.cn

Rongbin Zhou − *Key Laboratory of Immune Response and Immunotherapy, Institute of Health and Medicine, Hefei Comprehensive National Science Center, Hefei, Anhui 230026, China; Key Laboratory of Immune Response and Immunotherapy, School of Basic Medical Sciences, Division of Life Sciences and Medicine, University of Science and Technology of China, Hefei, Anhui 230026, China;* Email: zrb1980@ustc.edu.cn

Jie-Lou Liao − *Department of Chemical Physics, University of Science and Technology of China, Hefei, Anhui 230026, China;* orcid.org/0000-0003-1285-1067; Email: liaojl@ustc.edu.cn

Author

Haochen Xu − *Department of Chemical Physics, University of Science and Technology of China, Hefei, Anhui 230026, China*

Complete contact information is available at: https://pubs.acs.org/10.1021/acs.jcim.4c01112

Notes

The authors declare no competing financial interest.

■ ACKNOWLEDGMENTS

This work was funded by the National Natural Science Foundation of China under grant Nos. 2022YFA1303100 and 32090040. The authors thank Professor Hao Wu at Harvard Medical School for insightful discussions and sending us the PDB format coordinates (8ej4) of the active NLRP3 disk.

■ REFERENCES

(1) Swanson, K. V.; Deng, M.; Ting, J. P.-Y. The NLRP3 Inflammasome: Molecular Activation and Regulation to Therapeutics. *Nat. Rev. Immunol.* **2019**, *19* (8), 477−489.

(2) Huang, Y.; Xu, W.; Zhou, R. NLRP3 Inflammasome Activation and Cell Death. *Cell. Mol. Immunol.* **2021**, *18* (9), 2114−2127.

(3) Huang, Y.; Jiang, W.; Zhou, R. DAMP Sensing and Sterile Inflammation: Intracellular, Intercellular and Inter-Organ Pathways. *Nat. Rev. Immunol.* **2024**, DOI: 10.1038/s41577-024-01027-3.

(4) Fu, J.; Wu, H. Structural Mechanisms of NLRP3 Inflammasome Assembly and Activation. *Annu. Rev. Immunol.* **2023**, *41*, 301−316.

(5) Mangan, M. S. J.; Olhava, E. J.; Roush, W. R.; Seidel, H. M.; Glick, G. D.; Latz, E. Targeting the NLRP3 Inflammasome in Inflammatory Diseases. *Nat. Rev. Drug Discovery* **2018**, *17* (9), 588−606.

(6) Jiang, H.; Gong, T.; Zhou, R. The Strategies of Targeting the NLRP3 Inflammasome to Treat Inflammatory Diseases. *Adv. Immunol.* **2020**, *145*, 55−93.

(7) Tengesdal, I. W.; Menon, D. R.; Osborne, D. G.; et al. Targeting Tumor-Derived NLRP3 Reduces Melanoma Progression by Limiting MDSCs Expansion. *Proc. Natl. Acad. Sci. U.S.A.* **2021**, *118* (10), No. e2000915118.

(8) Chen, Y.; He, H.; Lin, B.; Chen, Y.; Deng, X.; Jiang, W.; Zhou, R. RRx-001 Ameliorates Inflammatory Diseases by Acting as a Potent Covalent NLRP3 Inhibitor. *Cell. Mol. Immunol.* **2021**, *18* (6), 1425−1436.

(9) Muñoz-Planillo, R.; Kuffa, P.; Martinez-Colon, G.; Smith, B. L.; Rajendiran, T. M.; Nunez, G. K^+ Efflux is the Common Trigger of NLRP3 Inflammasome Activation by Bacterial Toxins and Particulate Matter. *Immunity* **2013**, *38* (6), 1142−1153.

(10) Gong, T.; Yang, Y.; Jin, T.; Jiang, W.; Zhou, R. Orchestration of NLRP3 Inflammasome Activation by Ion Fluxes. *Trends Immunol.* **2018**, *39* (5), 393−406.

(11) Tapia-Abellán, A.; Angosto-Bazarra, D.; Alarcón-Vila, C.; Baños, M. C.; Hafner-Bratkovič, I.; Oliva, B.; Pelegrín, P. Sensing Low Intracellular Potassium by NLRP3 Results in a Stable Open Structure that Promotes Inflammasome Activation. *Sci. Adv.* **2021**, *7* (38), No. eabf4468.

(12) Schmid-Burgk, J. L.; Chauhan, D.; Schmidt, T.; Ebert, T. S.; Reinhardt, J.; Endl, E.; Hornung, V. A. Genome-Wide CRISPR (Clustered Regularly Interspaced Short Palindromic Repeats) Screen Identifies NEK7 as an Essential Component of NLRP3 Inflammasome Activation. *J. Biol. Chem.* **2016**, *291* (1), 103−109.

(13) He, Y.; Zeng, M. Y.; Yang, D.; Motro, B.; Núñez, G. NEK7 is An Essential Mediator of NLRP3 Activation Downstream of Potassium Efflux. *Nature* **2016**, *530* (7590), 354−357.

(14) Shi, H.; Wang, Y.; Li, X.; Zhan, X.; Tang, M.; Fina, M.; et al. NLRP3 Activation and Mitosis Are Mutually Exclusive Events Coordinated by NEK7, A New Inflammasome Component. *Nat. Immunol.* **2016**, *17* (3), 250−258.

(15) Li, X.; Thome, S.; Ma, X.; Amrute-Nayak, M.; Finigan, A.; Kitt, L.; et al. MARK4 Regulates NLRP3 Positioning and Inflammasome Activation through a Microtubule-dependent Mechanism. *Nat. Commun.* **2017**, *8*, No. 15986.
(16) Yang, X. D.; Li, W.; Zhang, S.; Wu, D.; Jiang, X.; Tan, R.; et al. PLK4 Deubiquitination by Spata2-CYLD Suppresses NEK7-Mediated NLRP3 Inflammasome Activation at the Centrosome. *EMBO J.* **2020**, *39* (2), No. e102201.
(17) Magupalli, V. G.; Negro, R.; Tian, Y.; Hauenstein, A. V.; Caprio, D. G.; et al. HDAC6Mediates an Aggresome-Like Mechanism for NLRP3 and Pyrin Inflammasome Activation. *Science* **2020**, *369* (6510), No. eaas8995.
(18) Sharif, H.; Wang, L.; Wang, W. L.; Magupalli, V. G.; Andreeva, L.; Qiao, Q.; Hauenstein, A. V.; Wu, Z.; Núñez, G.; Mao, Y.; Wu, H. Structural Mechanism for NEK7-Licensed Activation of NLRP3 Inflammasome. *Nature* **2019**, *570* (7761), 338−343.
(19) Andreeva, L.; David, L.; Rawson, S.; Shen, C.; Pasricha, T.; Pelegrin, P.; Wu, H. NLRP3 Cages Revealed by Full-Length Mouse NLRP3 Structure Control Pathway Activation. *Cell* **2021**, *184* (26), 6299−6312.e22.
(20) Hochheiser, I. V.; Pilsl, M.; Hagelueken, G.; Moecking, J.; Marleaux, M.; Brinkschulte, R.; Latz, E.; Engel, C.; Geyer, M. Structure of the NLRP3 Decamer Bound to the Cytokine Release Inhibitor CRID3. *Nature* **2022**, *604* (7904), 184−189.
(21) Ohto, U.; Kamitsukasa, Y.; Ishida, H.; Zhang, Z.; Murakami, K.; Hirama, C.; Maekawa, S.; Shimizu, T. Structural Basis for the Oligomerization-Mediated Regulation of NLRP3 Inflammasome Activation. *Proc. Natl. Acad. Sci. U.S.A.* **2022**, *119* (11), No. e2121353119.
(22) Xiao, L.; Magupalli, V. G.; Wu, H. Cryo-EM Structures of the Active NLRP3 Inflammasome Disc. *Nature* **2023**, *613* (7944), 595−600.
(23) Yu, X.; Matico, R. E.; Miller, R.; Schoubroeck, B. V.; Grauwen, K.; et al. Structural Basis for the Oligomerization Facilitated NLRP3 Activation. *Nat. Commun.* **2024**, *15* (1), No. 1164.
(24) Fu, J.; Schroder, K.; Wu, H. Mechanistic Insights from Inflammasome Structures. *Nat. Rev. Immunol.* **2024**, *24*, 518−535.
(25) Lindorff-Larsen, K.; Piana, S.; Palmo, K.; Maragakis, P.; Klepeis, J. L.; Dror, R. O.; Shaw, D. E. Improved Side-Chain Torsion Potentials for the Amber ff99SB Protein Force Field. *Proteins: Struct., Funct., Bioinf.* **2010**, *78*, 1950−1958.
(26) da Silva, A. W. S.; Vranken, W. F. ACPYPE-Antechamber Python Parser Interface. *BMC Res. Notes* **2012**, *5*, No. 367.
(27) Darden, T.; York, D.; Pedersen, L. Particle Mesh Ewald: An Nlog(N) Method for Ewald Sums in Large Systems. *J. Chem. Phys.* **1993**, *98* (12), 10089−10092.
(28) Hess, B.; Bekker, H.; Berendsen, H.; Fraaije, J. LINCS: A Linear Constraint Solver for Molecular Simulations. *J. Comput. Chem.* **1997**, *18* (12), 1463−1472.
(29) Miyamoto, S. P.; Kollman, A. Settle: An Analytical Version of the SHAKE and RATTLE Algorithm for Rigid Water Models. *J. Comput. Chem.* **1992**, *13* (8), 952−962.
(30) Abraham, M. J.; Murtola, T.; Schulz, R.; Pall, S.; Smith, J. C.; Hess, B.; Lindahl, E. GROMACS: High Performance Molecular Simulations through Multi-Level Parallelism from Laptops to Supercomputers. *SoftwareX* **2015**, *1-2*, 19−25.
(31) Bussi, G.; Donadio, D.; Parrinello, M. Canonical Sampling through Velocity Rescaling. *J. Chem. Phys.* **2007**, *126* (1), No. 014101.
(32) Evans, D. J.; Holian, B. L. The Nose−Hoover Thermostat. *J. Chem. Phys.* **1985**, *83* (8), 4069−4074.
(33) Parrinello, M.; Rahman, A. Polymorphic Transitions in Single Crystals: A New Molecular Dynamics Method. *J. Appl. Phys.* **1981**, *52*, 7182−7190.
(34) Kutzner, C.; Czub, J.; Grubmüller, H. Keep It Flexible: Driving Macromolecular Rotary Motions in Atomistic Simulations with GROMACS. *J. Chem. Theory Comput.* **2011**, *7* (5), 1381−1393.
(35) Kumar, S.; Bouzida, D.; Swendsen, R. H.; Kollman, P. A.; Rosenberg, J. M. The Weighted Histogram Analysis Method for Free-Energy Calculations on Biomolecules. I. The Method. *J. Comput. Chem.* **1992**, *13* (8), 1011−1021.
(36) Torrie, G. M.; Valleau, J. P. Nonphysical Sampling Distributions in Monte Carlo Free-Energy Estimation: Umbrella Sampling. *J. Comput. Phys.* **1977**, *23*, 187−199.
(37) Sheng, Y. J.; Yin, Y. W.; Ma, Y. Q.; Ding, Y. Q. Improving the Performance of MM/PBSA in Protein−Protein Interactions via the Screening Electrostatic Energy. *J. Chem. Inf. Model.* **2021**, *61* (5), 2454−2462.
(38) Wang, E.; Sun, H.; Wang, J.; et al. End-Point Binding Free Energy Calculation with MM/PBSA and MM/GBSA: Strategies and Applications in Drug Design. *Chem. Rev.* **2019**, *119* (16), 9478−9508.
(39) Duan, L.; Liu, X.; Zhang, J. Z. H. Interaction Entropy: A New Paradigm for Highly Efficient and Reliable Computation of Protein−Ligand Binding Free Energy. *J. Am. Chem. Soc.* **2016**, *138* (17), 5722−5728.
(40) Sun, Z.; Yan, Y. N.; Yang, M.; Zhang, J. Z. H. Interaction Entropy for Protein-Protein Binding. *J. Chem. Phys.* **2017**, *146* (12), No. 124124.
(41) Chen, C.; Yan, Z. S.; Ma, Y. Q.; Ding, H. M. Effect of Terahertz Waves on the Structure of the Aβ42 Monomer, Dimer, and Protofibril: Insights from Molecular Dynamics Simulations. *ACS Chem. Neurosci.* **2023**, *14* (23), 4128−4138.
(42) Jurrus, E.; Engel, D.; Star, K.; Monson, K.; Brandi, J.; Felberg, L. E.; Brookes, D. H.; Wilson, L.; Chen, J.; Liles, K.; et al. Improvements to the APBS Biomolecular Solvation Software Suite. *Protein Sci.* **2018**, *27* (1), 112−128.
(43) Wu, H. Higher-Order Assemblies in a New Paradigm of Signal Transduction. *Cell* **2013**, *153* (2), 287−292.

https://doi.org/10.1021/acs.jcim.4c01112
J. Chem. Inf. Model. 2024, 64, 6857−6865